Solar Physics (2006) 238: 377–390
DOI: 10.1007/s11207-006-0227-x 

# THE EFFECT OF THE HELIOSPHERIC CURRENT SHEET ON INTERPLANETARY SHOCKS

YANQIONG XIE
*State Key Laboratory of Space Weather, Center for Space Science and Applied Research, Chinese Academy of Sciences, Beijing 100080, China; Graduate School of the Chinese Academy of Sciences, Beijing 100049, China; Institute of Meteorology, PLA University of Science and Technology, Nanjing 211101, China*

and

FENGSI WEI, CHANGQING XIANG and XUESHANG FENG
*State Key Laboratory of Space Weather, Center for Space Science and Applied Research, Chinese Academy of Sciences, Beijing 100080, China*

(Received 23 May 2006; accepted 29 August 2006; Published online 9 November 2006)

**Abstract.** Using 180 interplanetary (IP) shock events associated with coronal mass ejections (CMEs) during 1997–2005, we investigate the influence of the heliospheric current sheet (HCS) upon the propagation and geoeffectiveness of IP shocks. Our preliminary results are: (1) The majority of CME-driving IP shocks occurred near the HCS. (2) The numbers of shock events and related geomagnetic storms observed when the Earth and the solar source are located on the same side of the HCS, represented by $f_{SS}$ and $f_{SG}$, respectively, are obviously higher than those when the Earth and the solar source are located on the opposite sides of the HCS, denoted by $f_{OS}$ and $f_{OG}$, with $f_{SS}/f_{OS} = 126/54$, $f_{SG}/f_{OG} = 91/36$. (3) Parameter jumps across the shock fronts for the same-side events are also higher than those for the opposite-side events, and the stronger shocks ($\Delta V \geq 200\,\mathrm{km\,s^{-1}}$) are mainly attributed to be same-side events, with $f_{SSh}/f_{OSh} = 28/15$, where $f_{SSh}$ and $f_{OSh}$ are numbers of stronger shocks which belong to same-side events and opposite-side events, respectively. (4) The level of the geomagnetic disturbances is higher for the same-side events than for the opposite-side events. The ratio of the number of intense magnetic storms ($\mathrm{Dst} < -100$) triggered by same-side events to those triggered by opposite-side events is 25/10. (5) We propose an empirical model to predict the arrival time of the shock at the Earth, whose accuracy is comparable to that of other prevailing models. These results show that the HCS is an important physical structure, which probably plays an important role in the propagation of interplanetary shocks and their geoeffectiveness.

## 1. Introduction

The Heliospheric Current Sheet (HCS) is the boundary encircling the Sun that separates oppositely directed magnetic fields originating from the Sun. It also represents the magnetic equator of the global heliosphere (Ness and Wilcox, 1964; Wilcox and Ness, 1965; Smith, 2001).

Since the HCS serves as a magnetic equator, many solar wind properties are organized with respect to it. Distributions of various plasma parameters, including solar wind speed, density, temperature, and composition, show a close correlation

with the HCS (Borrini *et al.*, 1981; Gosling *et al.*, 1981; Zhao and Hundhausen, 1981). Indeed, the latitudinal gradients of these and other parameters are best organized by heliomagnetic coordinates or distance from the HCS (see the review by Smith, 2001).

Such a special structure has attracted extensive attention from researchers who study the propagation of solar disturbances in the interplanetary space by means of data analyses and numerical simulations. As a result, plenty of data analyses were pursued in terms of the locations of solar sources in relation to the HCS in order to investigate the effect of the HCS on the propagation properties of solar disturbances (Henning, Scherrer, and Hoeksema, 1985; Wei, Zhang, and Huang, 1990; Wei, Liu, and Zhang, 1991). For instance, Henning, Scherrer, and Hoeksema (1985) found that flares on the same side of the HCS as the Earth tend to produce larger disturbances than those on the opposite side and suggested that this may be caused by the interaction between the disturbances and the slow wind plasma astride the HCS. On the other hand, the fastest propagation direction of IP shocks was found to deflect from the flare normal and drift toward the HCS in the meridional plane by Wei and Dryer (1991). They suggested that the deflection of the shock toward the HCS might be caused by the dynamic action of the near-Sun magnetic field.

Numerical simulations were also invoked to study the propagation of IP shocks in the presence of the HCS. Odstrčil, Dryer, and Smith (1996), Odstrčil, Smith, and Dryer (1996) and Smith, Odstrčil, and Dryer (1998) explored the effect of the HCS and heliospheric plasma sheet (HPS) on the shock propagation in terms of a 2.5-D MHD model in the meridional plane. These studies arrived at the conclusion that a dimple is formed at the forward shock front across the HPS and both the shock travel time to 1 AU and the shock properties are affected when the shock crosses the HPS. Hu and Jia (2001) found that the slow solar wind astride the HCS and HPS exerts a significant influence on the shock which is weakened in strength after its transmission. Leau (2004) used the HAF code to simulate CME events and showed that the ejected plasma and its driving IP shocks cannot permeate the sector boundary, but do interact with the sector boundary. The interactions will substantially change both the shape of the sector boundary and the shock arrival time at the Earth. Besides these numerical simulations, kinematic calculations carried out by Hakamada and Akasofu (1982) indicated that the HCS can play a substantial role in the propagation of geomagnetically effective shocks.

In this paper, we choose 180 IP shock events during 1997 – 2005 and study the effect of the HCS on the propagation of shocks and its geoeffectiveness by data analyses. The distributions of same-side events and opposite-side events and the parameter jumps across the IP shocks observed near the Earth are analyzed in Section 2. An empirical formula is proposed to predict shock arrival time at the Earth in Section 3, together with a statistical study to compare our predicted results with those of other prevalent models. In Section 4, the influence of the HCS on the geoeffectiveness

of IP shocks is presented. Finally, we conclude and summarize the paper in Section 5.

## 2. Statistics of Same-Side and Opposite-Side Events

### 2.1. Data selection

A list of CME-associated shocks is compiled using events reported in the literature (McKenna-Lawlor *et al.*, 2002; Cane and Richardson, 2003; Cho *et al.*, 2003; Fry *et al.*, 2003; Manoharan *et al.*, 2004; Schwenn *et al.*, 2005), supplemented with the shock list obtained from the Proton Monitor (PM) instrument on board the SOHO mission (available at *http://umtof.umd.edu/pm/*). We select 180 events (without any preference) represented in the above literature and website that occurred during the period from February 1997 to September 2005. These IP shock events cover a wide time range of nearly 9 years during the rising phase, solar maximum and the declining phase of Solar Cycle 23.

For each shock event, we need the following observational data: the location of the solar source, the initial time and speed of shock, the magnetic structure of the solar source surface (located at 2.5 solar radii), the IP shock and background solar wind observed by the spacecraft near the Earth, and the geomagnetic activity index, Dst. Some parameters, such as the start time and the initial speed of the shock and solar source position, are taken from the recognized results in aforementioned published papers and the helpful website. The synoptic chart of the magnetic field of the solar source on the surface are obtained from the Wilcox Solar Observatory at *http://quake.stanford.edu/∼wso/coronal.html*. Solar wind parameters near the Earth are determined from the data sets in the OMNI2 database (available at *http://omniweb.gsfc.nasa.gov/*). The geomagnetic activity index, Dst, is obtained from the World Data Center for Geomagnetism, Kyoto (*ftp://ftp.ngdc.noaa.gov/STP/GEOMAGNETIC_DATA/INDICES/*).

### 2.2. Distributions of same-side and opposite-side events

We first classify these 180 events into two categories according to the relative positions of the solar source and the Earth with respect to the HCS at the solar source on the surface: (1) same-side events, for which the solar source and the sub-Earth point are located on the same side of the HCS when the CME occurred; (2) opposite-side events, for which the solar source and the sub-Earth point are located on opposite sides of the HCS at the time of CME initiation. The examples of the two categories are shown in Figures 1(a) and (b), respectively.

Figure 2(a) shows the distribution of angular distance between the solar source and the HCS at the solar source on the surface. From this figure we can see that angular distances of 118 cases (66%) range between 0 and 30 degrees, which

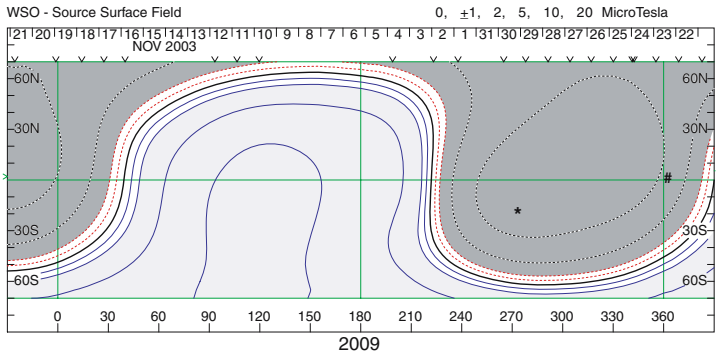


(a)

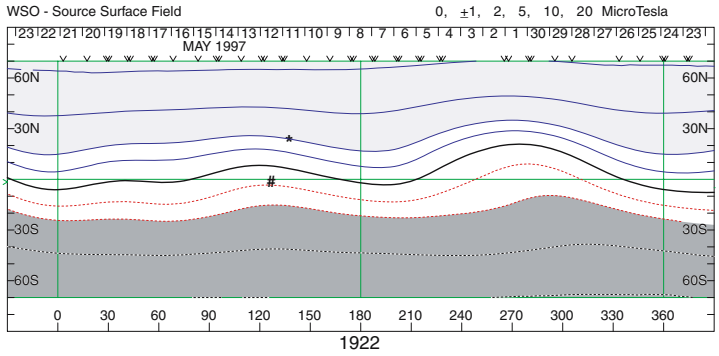


(b)

*Figure 1.* Schematic illustrations of same-side events and opposite-side events (the projections of the solar source and the Earth are marked by ⋆ and #, respectively): (a) An example of a same-side event (associated CME on 23 October 2003 08:54UT at S21E88); (b) An example of an opposite-side event (associated CME on 12 May 1997 05:30UT at N21W08).

indicates that the majority of solar sources are adjacent to the HCS. In addition, the number of events decreases sharply with an increase of the angular distance. That is to say, the physical conditions in the HCS and the surrounding areas are favorable for producing solar transient disturbance events, and that solar disturbance events occurring near the HCS can easily travel to the Earth.

If the position of the Earth is considered, the histogram of angular distance between the solar source and the HCS is plotted in Figure 2(b). The right-hand side of the figure presents the angular distance histogram for same-side events, and the left-hand side presents the angular distance histogram for opposite-side events. When the Earth and the solar source are located on the same side of the HCS, the number of shock events ($f_{\mathrm{SS}}$) is obviously higher than when they are on opposite sides ($f_{\mathrm{OS}}$), with $f_{\mathrm{SS}}/f_{\mathrm{OS}} = 126/54$. Furthermore, the general trend that the case number decreases with growing angular distance is obvious for both same-side events and opposite-side events. The maximum angular distance can

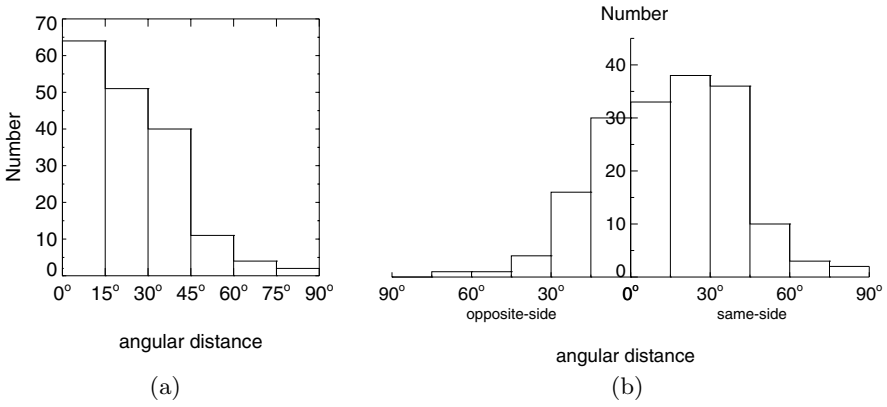


*Figure 2.* Histograms of the distributions of the angular distance between the solar source and the HCS: (a) without event classification; (b) with event classification.

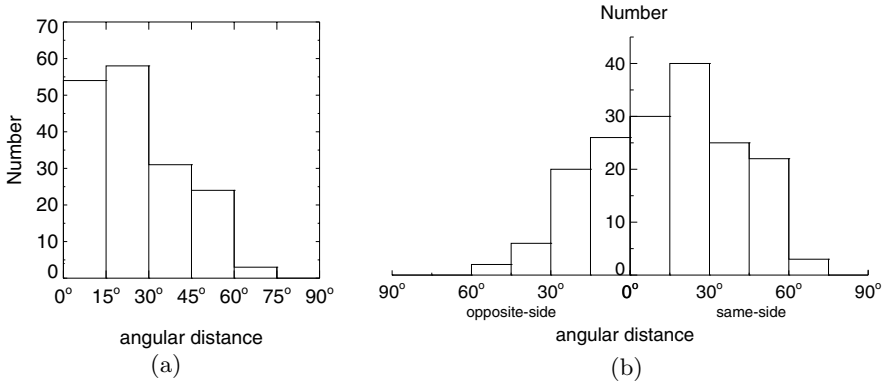


*Figure 3.* Histograms of the distributions of the angular distance between the Earth and the HCS: (a) without event classification; (b) with event classification.

reach 80 degrees for the same-side events and 75 degrees for the opposite-side events.

Similarly, the distributions of angular distance between the Earth and the HCS on the solar source surface are displayed in Figure 3(a). From the figure we can see that most shock events are observed when the Earth is located near the HCS. There are 117 cases (65%) lying in the angular distance range between 0 and 30 degrees. In addition, if the positions of the solar source are considered, and the histogram of angular distance between the Earth and the HCS is plotted in Figure 3(b), it is obvious that the number of same-side events is larger than that of opposite-side events. This implies that a same-side event can be observed by the spacecraft near the Earth more easily compared to an opposite-side event. The HCS between the solar source and the Earth may hinder an opposite-side event from traveling to the Earth.

To sum up, most of the selected CMEs occurred near the HCS. Same-side events (126 cases) can reach the Earth more easily compared to opposite-side events (only 54 cases).

### 2.3. SHOCK PARAMETERS NEAR 1AU

As we know, solar wind parameters will experience abrupt changes when crossing shock fronts. The magnitude of parameter jumps can be used to evaluate the strength of shock events. Here, we define parameter jumps across the shock front ($\Delta Q$) as $\Delta Q = \hat{Q} - \bar{Q}$, where $\bar{Q}$ is the daily mean value of a certain solar wind parameter on the day before the shock arrival, $\hat{Q}$ is the maximum value of the solar wind parameter of the shock arrival day and $Q$ can be solar wind speed ($V$), proton temperature ($T$), proton density ($N$) or the magnitude of the interplanetary magnetic field ($B$). On the basis of event classification mentioned in the previous section, comparisons of $\Delta Q$ between same-side shock events and opposite-side events are discussed below.

Figure 4 displays the distributions of $\Delta V$, $\Delta T$, $\Delta N$ and $\Delta B$ against the angular distance between the solar source and the HCS. Asymmetric distributions can be seen in this figure, which implies that shocks of the same-side category are more likely to arrive at the Earth than those of the opposite-side category. Furthermore, the stronger shocks with bigger $\Delta Q$ are restricted either to the same side or near the HCS location. A possible explanation may be that the HCS between the solar source and the Earth for an opposite-side event may hinder the shock from traveling to the Earth or weaken its strength, hence there are fewer opposite-side shocks. On the other hand, for same-side events, both stronger shocks and weaker shocks can reach the Earth easily without the hindrance of the HCS during the propagation of the shock.

Below, we choose $\Delta V$ as an indicator of shock strength. The quantitative analysis of the frequency number of the two kinds of shock events according to the different intervals of $\Delta V$, is listed in Table I. It is clear that most of the stronger shock events, with bigger $\Delta V$, belong to the same-side category. For example, for the shocks with

TABLE I

Statistics of same-side and opposite-side shock events by $\Delta V$.

| Intervals of $\Delta V$(km s$^{-1}$) | Ratio of number between same-side and opposite-side shock |
|---|---|
| $\Delta V < 100$ | 55:28 |
| $100 \leq \Delta V < 200$ | 43:11 |
| $200 \leq \Delta V < 300$ | 18:10 |
| $300 \leq \Delta V < 400$ | 04:04 |
| $\Delta V \geq 400$ | 06:01 |

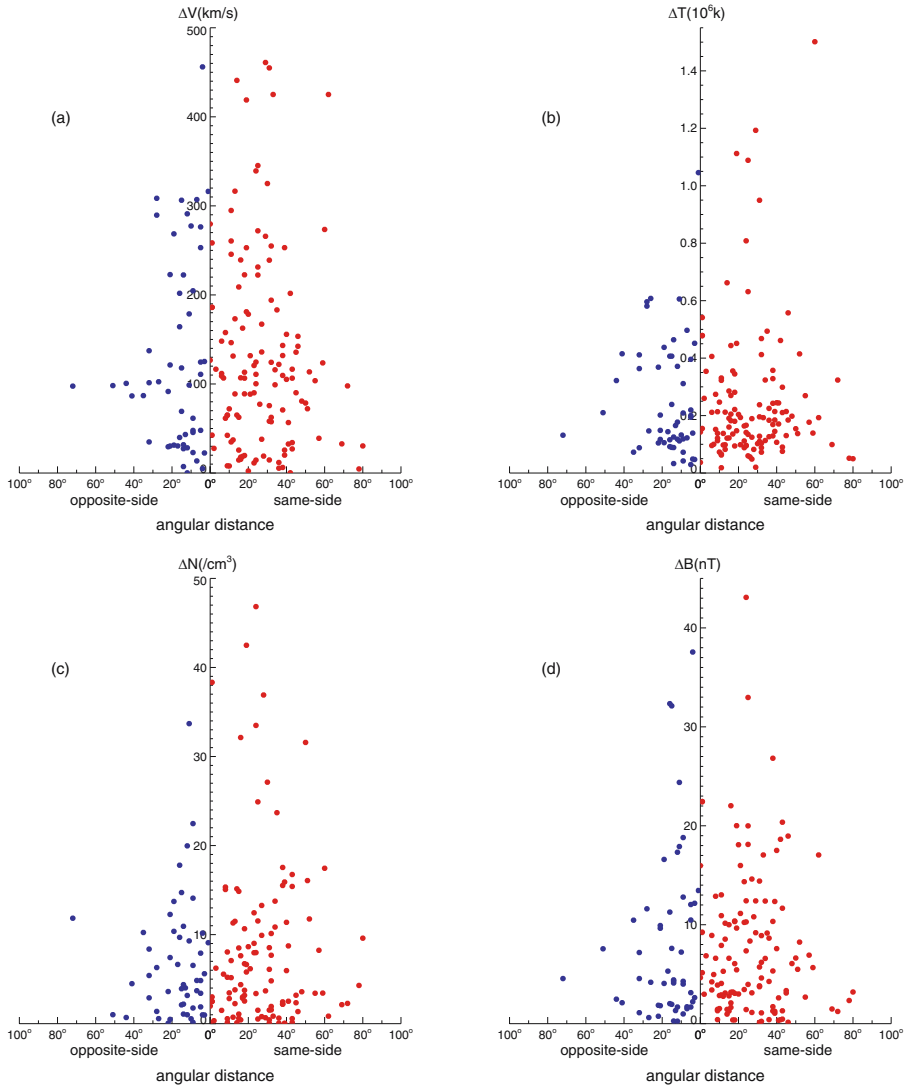


*Figure 4.* Distributions of parameter jumps across shock fronts with respect to the angular distance between the solar source and the HCS: (a) $\Delta V$, (b) $\Delta T$, (c) $\Delta N$, (d) $\Delta B$.

$\Delta V$ larger than 200 and 400 km s$^{-1}$, the ratios of same-side cases to opposite-side cases are 28/15 and 6/1, respectively.

## 3. Effect of HCS on Shock Arrival Time

Some numerical simulations have drawn the conclusion that the shock travel time to 1 AU and the shock properties at 1 AU are affected when the HCS is in the

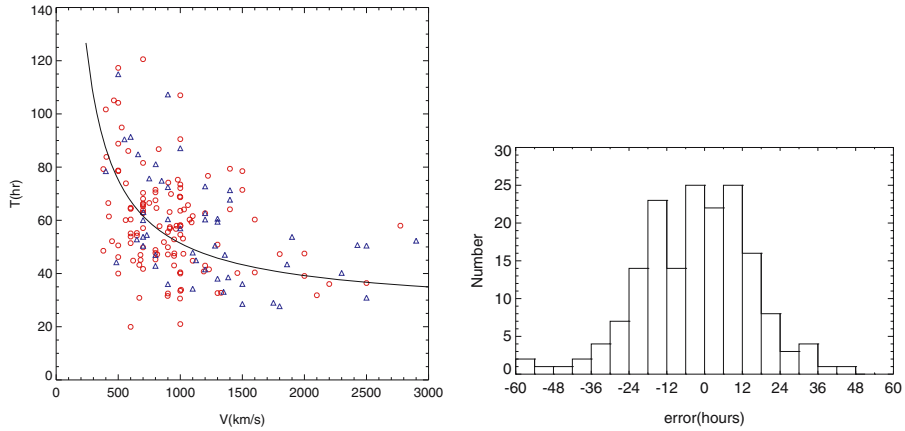


*Figure 5.* (a) Transit time of interplanetary shocks versus their initial speed (○ indicates a same-side event, △ indicates an opposite-side event). The *solid line* is a curvilinear fit to the data points. (b) Histograms showing the difference between predicted and observed times for the Solar-IP shock model using 6-h bins.

path of shock propagation (Smith, Odstrčil, and Dryer, 1998; Leau, 2004). They demonstrated that, qualitatively speaking, the existence of the HCS can affect the shock arrival time. However, how to quantify the degree of impact on shock travel time is an open problem.

In this paper, we define the transit time of an IP shock to be the time difference between the appearance of the CME in the LASCO/C2 field of view and the arrival of the shock in-situ, observed by spacecraft near the Earth. Figure 5(a) shows the shock transit time versus the shock initial speed, for same-side events (○) and opposite-side events (△), respectively. In this figure, the transit times are scattered over a large range from about 20 to 121 h. To illustrate the general characteristics of the relationship between the shock initial speed and the transit time, we fit these data using a comparatively simple formula (hereafter Solar-IP shock model), which gives a mean absolute error of 14.1 h for these 180 shocks.

$$T = 27.96 - 2.96 \times 10^{-4} V + 23710/V, \tag{1}$$

where $T$ (h) is the transit time and $V$ (km s$^{-1}$) is the initial speed of the shock. Figure 5(b) presents the time difference distribution between the predicted and observed transit times for the Solar-IP shock model. The errors are concentrated in a window of $\pm 18$ h.

In order to estimate the prediction accuracy of the model proposed here, we compare the performance of two types of Sun–Earth connection models: (1) an ensemble of shock propagation models (STOA, STOA-2, ISPM and HAFv.2), (2) empirical CME or shock propagation models (CME-ICME, CME-IP shock and

TABLE II

Number of correct predictions and the prediction errors for each model[a].

| | STOA | STOA-2 | ISPM | HAFv.2 | CME-ICME | CME-IP shock | Solar-IP shock |
|---|---|---|---|---|---|---|---|
| No. ($\leq\pm60$ h)[b] | 34 | 38 | 26 | 37 | 22 | 22 | 38 |
| Percentage | 89% | 100% | 68% | 97% | 58% | 58% | 100% |
| RMS ($\Delta T$)[c] | 18.9 | 18.3 | 20.3 | 21.6 | 17.3 | 18.6 | 18.5 |
| Mean ($\Delta T$)[d] | 14.5 | 14.4 | 15.8 | 16.3 | 15.0 | 14.5 | 15.3 |
| No. ($\leq\pm24$ h)[b] | 27 | 30 | 19 | 29 | 18 | 17 | 33 |
| Percentage | 71% | 79% | 50% | 76% | 47% | 45% | 87% |
| RMS ($\Delta T$) | 12.8 | 11.7 | 11.6 | 12.0 | 12.6 | 11.4 | 14.1 |
| Mean ($\Delta T$) | 10.5 | 9.7 | 9.4 | 9.9 | 11.6 | 9.2 | 12.2 |
| No. ($\leq\pm12$ h)[b] | 16 | 21 | 12 | 18 | 11 | 11 | 16 |
| Percentage | 42% | 55% | 32% | 47% | 29% | 29% | 42% |
| RMS ($\Delta T$) | 6.9 | 6.9 | 6.1 | 6.4 | 8.7 | 6.0 | 6.9 |
| Mean ($\Delta T$) | 6.0 | 6.0 | 5.0 | 5.4 | 8.2 | 4.9 | 5.9 |

[a]The prediction results of STOA, STOA-2, ISPM, HAFv.2, CME-ICME and CME-IP shock models are taken from the paper written by Cho *et al*. (2003).
[b]No. ($\leq\pm60/24/12$h) is the number of events that are predicted by these models within chosen windows of $\pm60$, $\pm24$ and $\pm12$ h, respectively.
[c]RMS ($\Delta T$) indicates the root-mean-square error.
[d]Mean ($\Delta T$) indicates the mean error.

Solar-IP shock). For details of the other five models, we refer the reader to the paper by Cho *et al*. (2003) and references therein. Here, we apply these models to 38 near-simultaneous CME and metric type II burst events, which can reasonably be taken to be associated with specific solar flares, listed in the paper by Cho *et al*. (2003). These 38 cases are a subset of our 180 events. Major results listed in Table II can be summarized as follows:

1. For the adopted window of $\pm24$ h, the success rates are found to be about 69% for the ensemble of shock propagation models, 47% for the CME-ICME model, 45% for the CME-IP shock model and 87% for our Solar-IP shock model. The estimated mean error of the shock arrival time within the same window is 9.9 h for the ensemble of shock propagation models, 11.6 h for the CME-ICME model, 9.2 h for the CME-IP shock model and 12.2 h for the Solar-IP shock model.
2. For the adopted window of $\pm12$ h, the success rates are found to be about 44% for the ensemble of shock propagation models, 29% for the CME-ICME model and the CME-IP shock model, and 42% for our Solar-IP shock model. The estimated mean error of the shock arrival time within the same window is 5.6 h

for the ensemble of shock propagation models, 8.2 h for the CME-ICME model, 4.9 h for the CME-IP shock model and 5.9 h for the Solar-IP shock model.

Summing up, the performance of our Solar-IP shock model is comparable to the other models in terms of their prediction errors, though each model has its own advantages and disadvantages.

Taking the categories of same-side event and opposite-side event into consideration, we have tried to predict shock arrival times by using functions similar to equation (1). However, the analysis results (details are omitted here) indicate that the prediction efficiency of such a classified forecast is not obviously better than that of an unclassified forecast. Figure 5(a) also shows that there is no systematic difference in shock arrival time between same-side and opposite-side events. Taking shock events with the same initial speed for example, the transit time of same-side cases is not generally lower than that of opposite-side events. In fact, the propagation of a shock is a complicated process. It may be affected by the process of shock generation, the conditions in the solar-terrestrial space, and some other related physical processes. Though some research results proved that the existence of the HCS could affect the arrival time of the shock, classified forecasts mentioned above can not successfully take this effect into consideration. Thus, in order to predict the shock arrival time more accurately, we should study the propagation of shocks thoroughly, improve the ground-based and space-borne observations and choose proper methods of analysis.

## 4. Influence of HCS upon Geoeffectiveness of Shock

Interplanetary shocks are an important means of energy transmission from the Sun to the Earth, resulting in geomagnetic activity (Gonzalez, Tsurutani, and Clúa de Gonzalez, 1999). Echer and Gonzalez (2004) studied the geoeffectiveness of interplanetary shock waves, magnetic clouds, heliospheric current sheet sector boundary crossings, and the combinations of these interplanetary structures. They found that around 57% of IP shocks, 60% of IP shocks at sector boundaries and 100% of magnetic clouds driving shocks and located at sector boundaries are geoeffective. The combination of high speed clouds driving shocks at sector boundaries could be particularly geoeffective, perhaps due the presence of multiple southward interplanetary magnetic field (IMF) structures, which could be due to the sector boundary crossing deflected fields, sheath and ejecta fields.

In this section, the geoeffectiveness of these selected IP shocks is evaluated through the Dst minimum value after the arrival of the structure. Figure 6(a) shows the Dst versus the angular distance between the Earth and the HCS, and Figure 6(b) is the distribution of Dst considering the classification of same-side and opposite-side events. In addition, the details of geoeffectiveness of same-side and opposite-side events are quantitatively listed in Table III. Major results from this study can be summarized as follows:

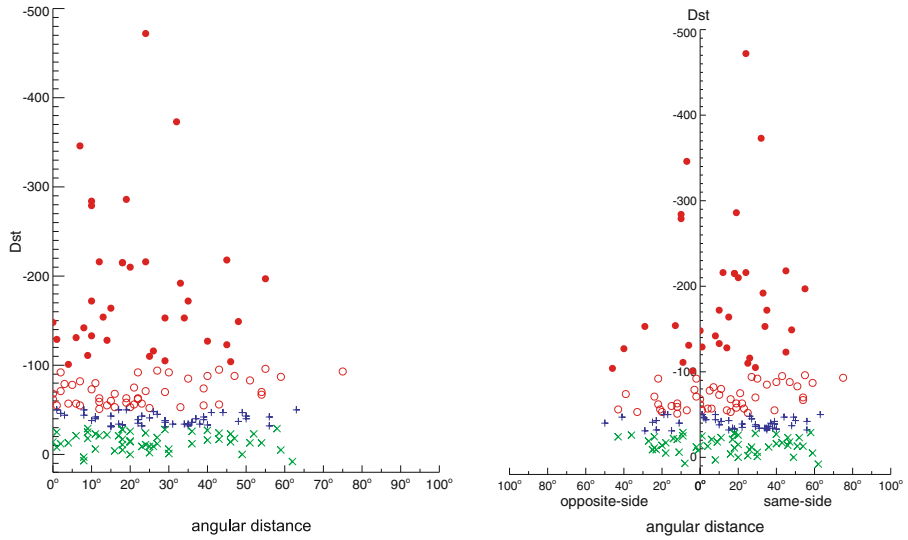


*Figure 6.* Dst index versus the angular distance between the Earth and the HCS (symbol • indicates an intense geomagnetic storm, ○ indicates a moderate geomagnetic storm, + indicates a weak geomagnetic storm and × indicates no geomagnetic storm): (a) without event classification; (b) with event classification.

1. From Figure 6(a), it is found that most geomagnetic storms, especially intense storms, which are supposedly associated with CME-producing IP shocks, occur when the Earth is close to the HCS. This is in agreement with the results of Mendoza and Pérez Enríquez (1993, 1995), who found that CMEs tend to accumulate around the heliomagnetic equator.
2. From Figure 6(b), the distribution of Dst presents obvious asymmetry if considering event classification. Just as the statistical results listed in Table III, the number of weak storms associated with same-side events and opposite-side events are 34 and 10, respectively; for moderate storms, the numbers are 32 and 16; and for intense storms, the numbers are 25 and 10, respectively. To sum up, of all these 127 geomagnetic storms (excluding the 53 cases without storms), 91 storms resulted from same-side events, while only 36 storms resulted from opposite-side events. From another point of view, about 72% (91/126) of same-side events and 67% (36/54) of opposite-side events, respectively, induce geomagnetic storms above weak storm level.
3. The majority of geomagnetic disturbances, especially intense storms, are triggered by same-side events. These obvious differences of distributions between the two categories for both Dst index and the shock parameter $\Delta Q$ (shown in Figure 4) are similar, which indicates that the geomagnetic disturbances are closely related to the corresponding interplanetary disturbances.

TABLE III
Statistics of geoeffectiveness of same-side and opposite-side shocks.

| | Same-side | Opposite-side | Total |
|---|---|---|---|
| Number of no storm ($Dst \geq -30$) | 35 | 18 | 53 |
| Number of weak storm ($-50 \leq Dst < -30$) | 34 | 10 | 44 |
| Number of moderate storm ($-100 \leq Dst < -50$) | 32 | 16 | 48 |
| Number of intense storm ($Dst < -100$) | 25 | 10 | 35 |
| Total | 126 | 54 | 180 |

From discussions above, it is reasonable to say that the HCS is an important structure for studying the geoeffectiveness of IP shocks. Mendoza and Pérez Enríquez (1995) have even studied the distribution of storm sudden commencements (SSCs) and their associated geomagnetic activity with respect to the Earth's crossing of the HCS. They found that most SSC events occur when the Earth is close to the current sheet. However, they found that the geoeffectiveness of SSCs seems to be independent of their position with respect to the HCS.

It should be noted that, however, besides the same-side and opposite-side effects, many other key factors must also be considered when predicting geomagnetic disturbances quantitatively, such as angular distances between the solar source, the Earth and the HCS, the southward component of the IMF, and the quite different situations near the terrestrial space for each event. Yermolaev *et al*. (2005) also suggested that both different analysis methods used in each of three areas (solar atmosphere, IP space and geomagnetosphere) and a way to compare the phenomena in various space areas or to trace data in different directions are of great importance to researching the entire chain of solar-terrestrial physics.

## 5. Conclusions and Summary

The HCS is an important physical structure to study the propagation and geoeffectiveness of IP shocks. Based on the analysis of observational data, the following conclusions are obtained:

(1) The areas on the Sun around the HCS are preferential places where transient ejections of coronal material (CMEs) occur.
(2) The majority of the 180 CME-IP shock events belong to the same-side category.
(3) For same-side events, not only the stronger IP shock but also the weaker shock can be observed near the Earth more easily compared to opposite-side events. Maybe the HCS in the path of opposite-side shock events could impede their propagation and weaken them.

(4) The existence of the HCS may affect the shock arrival time at the Earth. An empirical formula is obtained to predict shock arrival time with the shock initial speed as input.
(5) The intensity of geomagnetic activity generally declines with an increase of angular distance between the Earth and the HCS. Most geomagnetic storms are focused on the same side. In addition, same-side events tend to produce larger disturbances than opposite-side events.

These results are meaningful in the field of space weather. How to apply them to predict the arrival time of the shock and its geoeffectiveness is a subject worthy of further study.

## Acknowledgements

This work is jointly supported by the National Natural Science Foundation of China (Grant Nos. 40536029, 40336053 and 40374056) and the International Collaboration Research Team Program of the Chinese Academy of Sciences.

## References

Borrini, G., Wilcox, J.M., Gosling, J.T., Bame, S.J., and Feldman, W.C.: 1981, *J. Geophys. Res.* **86**, 4565.
Cane, H.V. and Richardson, I.G.: 2003, *J. Geophys. Res.* **108**(A4), 1156.
Cho, K.-S., Moon, Y.-J., Dryer, M., Fry, C.D., Park, Y.-D., and Kim, K.-S.: 2003, *J. Geophys. Res.* **108**(A12), 1445.
Echer, E. and Gonzalez, W.D.: 2004, *Geophys. Res. Lett.* **31**, L09808.
Fry, C.D., Dryer, M., Smith, Z., Sun, W., Deehr, C.S., and Akasofu, S.-I.: 2003, *J. Geophys. Res.* **108**(A2), 1070.
Gonzalez, W.D., Tsurutani, B.T., and Clúa de Gonzalez, A.L.: 1999, *Space Sci. Rev.* **88**, 529.
Gosling, J.T., Asbridge, J.R., Bame, S.J., Feldman, W.C., Borrini, G., and Hansen, R.T.: 1981, *J. Geophys. Res.* **86**, 5438.
Hakamada, K. and Akasofu, S.-I.: 1982, *Space Sci. Rev.* **31**, 3.
Henning, H.M., Scherrer, P.H., and Hoeksema, J.T.: 1985, *J. Geophys Res.* **90**(A11), 11055.
Hu, Y.Q. and Jia, X.Z.: 2001, *J. Geophys. Res.* **106**(A12), 29229.
Leau, W.K.: 2004, Graduation thesis for master degree of Institute of Space Science National Center University, Taiwan.
Manoharan, P.K., Gopalswamy N., Yashiro, S., Lara, A., Michalek, G., and Howard, R.A.: 2004, *J. Geophys. Res.* **109**(A6), A06109.
McKenna-Lawlor, S.M.P., Dryer, M., Smith, Z., Kecskemety, K., Fry, C.D., Sun, W., Deehr, C.S., Berdichevsky, D., Kudela, K., and Zastenker, G.: 2002, *Ann. Geophys.* **20**, 917.
Mendoza, B. and Pérez Enríquez, R.: 1993, *J. Geophys. Res.* **98**, 9365.
Mendoza, B. and Pérez Enríquez, R.: 1995, *J. Geophys. Res.* **100**, 7877.
Ness, N.F. and Wilcox, J.M.: 1964, *Plasma Rev. Lett.* **13**, 461.
Odstrčil, D., Dryer, M., and Smith, Z.: 1996, *J. Geophys. Res.* **101**, 19973.
Odstrčil, D., Smith, Z., and Dryer, M.: 1996, *Geophys. Res. Lett.* **23**, 2521.

Schwenn, R., Dal Lago, A., Huttunen, E., and Gonzalez, W.D.: 2005, *Ann. Geophys.* **23**, 1033.
Smith, Z., Odstrčil, D., and Dryer, M.: 1998, *J Geophys. Res.* **103**(A9), 20581.
Smith, E.J.: 2001, *J. Geophys. Res.* **106**(A8), 15819.
Wei, F.S. and Dryer, M.: 1991, *Solar Phys.* **132**, 373.
Wei, F.S., Liu, S.Q., and Zhang, J.H.: 1991, *Acta Geophys. Sinica* **34**, 133.
Wei, F.S., Zhang, J.H., and Huang, S.P.: 1990, *Acta Geophys. Sinica* **33**, 125.
Wilcox, J.M. and Ness, N.F.: 1965, *J. Geophys. Res.* **70**, 5793.
Yermolaev, Y.I., Yermolaev, M.Y., Zastenker, G.N., Zelenyi, L.M., Petrukovich, A.A., and Sauvaud J.-A.: 2005, *Planetary Space Sci.* **53**, 189.
Zhao, X.P. and Hundhausen, A.J.: 1981, *J. Geophys. Res.* **86**, 5423.